Prepared for submission to JCAP

Biases on cosmological parameter estimators from galaxy cluster number counts

M. Penna-Lima[a,b] **M. Makler,**[b] **C. A. Wuensche**[a]

[a]Instituto Nacional de Pesquisas Espaciais, Divisão de Astrofísica,
Av. dos Astronautas 1758, 12227-010, São José dos Campos – SP, Brazil
[b]Centro Brasileiro de Pesquisas Físicas,
Rua Dr. Xavier Sigaud 150, 22290-180, Rio de Janeiro – RJ, Brazil

E-mail: mariana.lima@inpe.br, martin@cbpf.br, ca.wuensche@inpe.br

Abstract. Sunyaev-Zel'dovich (SZ) surveys are promising probes of cosmology - in particular for Dark Energy (DE) -, given their ability to find distant clusters and provide estimates for their mass. However, current SZ catalogs contain tens to hundreds of objects and maximum likelihood estimators may present biases for such sample sizes. In this work we study estimators from cluster abundance for some cosmological parameters, in particular the DE equation of state parameter w_0, the amplitude of density fluctuations σ_8, and the Dark Matter density parameter Ω_c. We begin by deriving an unbinned likelihood for cluster number counts, showing that it is equivalent to the one commonly used in the literature. We use the Monte Carlo approach to determine the presence of bias using this likelihood and study its behavior with both the area and depth of the survey, and the number of cosmological parameters fitted. Our fiducial models are based on the South Pole Telescope (SPT) SZ survey. Assuming perfect knowledge of mass and redshift some estimators have non-negligible biases. For example, the bias of σ_8 corresponds to about 40% of its statistical error bar when fitted together with Ω_c and w_0. Including a SZ mass-observable relation decreases the relevance of the bias, for the typical sizes of current SZ surveys. Considering a joint likelihood for cluster abundance and the so-called "distance priors", we obtain that the biases are negligible compared to the statistical errors. However, we show that the biases from SZ estimators do not go away with increasing sample sizes and they may become the dominant source of error for an all sky survey at the SPT sensitivity. Finally, we compute the confidence regions for the cosmological parameters using Fisher matrix and profile likelihood approaches, showing that they are compatible with the Monte Carlo ones. The results of this work validate the use of the current maximum likelihood methods for present SZ surveys, but highlight the need for further studies for upcoming experiments. To perform the analyses of this work, we developed fast, accurate, and adaptable codes for cluster counts in the framework of the Numerical Cosmology Library.

Keywords: cluster counts, cosmological parameters from LSS

ArXiv ePrint: 1312.4430

Contents

1 Introduction

The abundance of galaxy clusters and their spatial distribution as functions of redshift and mass provide strong constraints on the matter density parameter Ω_m and the amplitude of the matter power spectrum σ_8 [1–5]. For high redshift surveys ($z > 1.0$), clusters are also powerful tools to study Dark Energy (DE) since they depend on the linear growth of density perturbations and the comoving volume [2, 6] (for a review see [7] and references therein). The coming years are promising for cluster cosmology in view of surveys which will provide deep and large catalogs such as the Dark Energy Survey (DES) [8] and the forthcoming Large Synoptic Survey Telescope (LSST) [9] optical surveys. The ongoing Sunyaev-Zel'dovich (SZ) surveys carried by the South Pole Telescope (SPT) [10–12], the Atacama Cosmology Telescope (ACT) [13] and the Planck probe [14] have already yielded catalogs with massive clusters and redshifts up to 1.5.

The number density of Dark Matter (DM) halos as a function of redshift and mass are modeled using a combination of analytical and numerical results. Although the massive DM halos are identified as galaxy clusters, their masses are not directly observable. It is necessary to use observable quantities, such as the X-ray temperature [15] or SZ flux decrement [10], to obtain mass-observable scaling relations (for a review, see [16]). The combination of a mass proxy with a theoretical model can be used to predict the number density of galaxy clusters. Therefore, the success of cluster cosmology relies on a good description of cluster counts and clustering, both based on a cosmological model and high-quality observations.

It is known that uncertainties arising from both mass-observable relations and photometric redshifts degrade constraints on cosmological parameters [17, 18]. These uncertainties comprehend both statistical and systematic errors. Other sources of uncertainties are sample-variance and shot-noise (due to the discreteness of the clusters). Optical surveys provide large catalogs (tens of thousand clusters) and, therefore, the shot-noise contribution is negligible with respect to sample-variance, which dominates along with mass uncertainties. On the other hand, X-ray and SZ catalogs contain only tens to hundreds objects. However, they usually have better mass estimates, higher completeness and purity, for example. In this case the cosmological analyses are shot-noise dominated.

Usually the cluster likelihood function is built taking into account the error sources mentioned above. Nevertheless, it is assumed that cosmological parameter estimators do not yield extra uncertainties. The Maximum Likelihood (ML) method is extensively used to estimate the values of parameters given a data set. ML estimators are usually consistent, i.e., the expected value of a parameter tends to its true value when the size of the data sample (n) is sufficiently large, and asymptotically efficient, i.e., the variance of the estimator attains the minimum variance bound as $n \to \infty$. However, ML estimators are not necessarily unbiased and, even if they are consistent, in practical cases the data sample sizes may not be large enough to guarantee that the asymptotic limit is reached [19–22].[1]

In this work, we study some cosmological parameter estimators in the context of SZ surveys, specifically from the SPT. For the redshift and mass ranges of SPT catalogs, sample variance is negligible [15, 23]. Therefore, we build the likelihood only for the cluster number counts and do not include the spatial clustering. We introduce a formalism to build this likelihood and show that it is similar to the one commonly used in the literature, in the limit where there is only one object in each bin of redshift and mass. To study the estimators, we use the Monte Carlo approach which consists on randomly sampling artificial data sets from a distribution numerous times.

To perform this work it was necessary to develop fast and accurate codes. These were implemented in the *Numerical Cosmology* Library (NumCosmo) [24] framework, which is open source and adaptable to new models and data, including several cosmological observables.

This paper is organized as follows. In section 2 we present the model and assumptions used to compute the halo number counts. In section 3, we introduce an unbinned likelihood for this observable and compare it with the standard one used in the literature. Then we describe the methodology to compute the bias of an estimator (section 4) and apply it using the likelihood for DM halo abundance (section 5). In section 6 we study the biases on the cosmological parameter estimators using a SZ mass-observable relation and investigate their dependence on the combination of free parameters fitted and the survey area and depth. We also include the photometric redshift uncertainty. In section 7 we analyse cosmological

[1] A common example is the variance ML estimator of a Gaussian distribution with mean $\bar{x}$, $\sigma^2_{ML} = \frac{1}{N}\sum_{i=1}^{N}(x_i - \bar{x})^2$, which is biased. The unbiased estimator is given by $\sigma^2 = \frac{1}{(N-1)}\sum_{i=1}^{N}(x_i - \bar{x})^2$.

parameter estimators obtained from a joint likelihood of cluster number counts and cosmic microwave background data. Finally, in section 8, we compare some estimator error bars computed using three different statistical methods: Monte Carlo, Fisher matrix and profile likelihood. Our concluding remarks are presented in section 9.

2 Cluster number counts

The mean number of dark matter halos with mass in the range $[M, M + dM]$ and in the redshift interval $[z, z + dz]$ is given by

$$\frac{d^2N}{dz d\ln M} dz d\ln M = \frac{dV}{dz}\frac{dn(M,z)}{d\ln M} dz d\ln M, \tag{2.1}$$

where $\frac{dn(M,z)}{d\ln M}$ is the comoving number density of halos at redshift z with mass M (i.e., the mass function). Assuming a homogeneous and isotropic universe and, as indicated by current observational data, spatially flat, the comoving volume element is

$$\frac{dV}{dz} = \Delta\Omega \left(\frac{\pi}{180}\right)^2 \frac{c}{H(z)} \left(\int_0^z dz' \frac{c}{H(z')}\right)^2, \tag{2.2}$$

where $\Delta\Omega$ is the survey area in square degrees. In this paper, we assume a constant DE equation of state parameter $p_{DE}/\rho_{DE} = w_0$, such that the Hubble function is

$$H(z) = H_0 \left[\Omega_r (1+z)^4 + \Omega_m (1+z)^3 + \Omega_{DE} (1+z)^{3(1+w_0)}\right]^{1/2}, \tag{2.3}$$

where H_0 is the Hubble constant. The energy density parameters Ω_x are the ratio between the energy density $\rho_x(z=0)$ and the critical energy density $\rho_{crit} = \frac{3H_0^2}{8\pi G}$. In eq. (2.3) Ω_r, Ω_m, and Ω_{DE} are the radiation, matter, and DE density parameters, respectively. As we are assuming a flat universe, $\Omega_{DE} = 1 - \Omega_m - \Omega_r$.

The mass function can be written as [25–27]

$$\frac{dn(M,z)}{d\ln M} = -\frac{\rho_m(z)}{M} f(\sigma_R, z) \frac{1}{\sigma_R}\frac{d\sigma_R}{d\ln M}, \tag{2.4}$$

where $\rho_m(z)$ is the mean matter density at redshift z, $f(\sigma_R, z)$ is the so called multiplicity function, which contains information about the nonlinear regime of halo formation, and σ_R^2 is the variance of the linear density contrast filtered on the length scale R associated to the mass M:

$$\sigma_R^2(z) = \int_0^\infty \frac{dk}{2\pi^2} k^2 P(k,z) |W(k,R)|^2, \tag{2.5}$$

where $W(k,R)$ is the window function and $P(k,z)$ is the linear power spectrum. In particular, we use the spherical top-hat function whose Fourier transform is

$$W(k,R) = \frac{3}{(kR)^3}(\sin kR - (kR)\cos kR), \tag{2.6}$$

and encloses a mass $M = 4\pi\rho_m R^3/3$.

The linear power spectrum is given by

$$P(k,z) = A\, k^{n_s}\, T(k)^2\, D(z)^2, \tag{2.7}$$

where n_s is the spectral index, $D(z)$ is the linear growth function, and $T(k)$ is the transfer function. In this paper, we use the Eisenstein-Hu (EH) [28] fitting function for $T(k)$.[2] The power spectrum normalization A may be written in terms of the standard deviation of the density contrast at a scale $R = 8h^{-1}$Mpc, σ_8:

$$A = \frac{\sigma_8^2}{\int_0^\infty \frac{dk}{2\pi^2} k^{(n_s+2)} T(k)^2 W^2(k,8)}. \tag{2.8}$$

In this work we compute $D(z)$ by numerically solving the differential equation for the growing mode of linear perturbations [30, 31],

$$\frac{d^2D}{dz^2} - \left(\frac{1}{1+z} - \frac{1}{E(z)}\frac{dE(z)}{dz}\right)\frac{dD}{dz} = \frac{3\Omega_m}{2E^2(z)}(1+z)D, \tag{2.9}$$

where we defined the normalized Hubble function as $E(z) = H(z)/H_0$ and $D(z)$ is normalized to unity at $z = 0$.

The first functional form for $f(\sigma)$ was obtained analytically by Press & Schechter assuming the spherical collapse of initial density peaks [25]. The multiplicity function was shown to be *universal*, in the sense that it does not depend on the cosmological parameters nor the initial conditions. A semi-analytic expression for $f(\sigma)$ was obtained by Sheth & Tormen [27] considering an ellipsoidal collapse approximation and a statistical treatment using a moving barrier. Their results were shown to be in broad agreement with cosmological N-body simulations. This motivated multiplicity functions to be fitted directly from the simulations [32–34], providing more accurate fitting functions. In addition, the universality property was verified to a good approximation in the simulations. In this work, we use the Tinker et al. [34] multiplicity function given by

$$f(\sigma_R(z), z) = A\left[\left(\frac{\sigma_R(z)}{b}\right)^{-a} + 1\right]\exp(-c\sigma_R^{-2}(z)), \tag{2.10}$$

where the values of the parameters A, a, b, and c depend on the redshift and halo mass definition. To allow for a more direct comparison with SZ data, we consider the mass contained in a spherical region 500 times the critical density at z, i.e., $R_\Delta = (3M_\Delta/4\pi\Delta\rho_{crit})^{1/3}$, with $\Delta = 500$. Reference [34] provides values for the mass function parameters for various values of Δ. Following their recommendation, we use spline interpolation to obtain these parameters for $\Delta = 500$ to a good accuracy. It is worth noting that, in our analyses, we neglect uncertainties related to the determination of the multiplicity function. In particular, we ignore the errors on the fitted parameters A, a, b and c. In reference [35] the authors show that while errors of the order of 10% in the mass function degrade the constraints on cosmological parameters, this effect is small when compared with that of the mass-observable relation.

3 Likelihood Model

In this section, we review the standard likelihood employed in the literature for halo abundance and introduce one based on the Extended Maximum Likelihood method.[3] We show that these

[2] We have checked that using the transfer function from CAMB [29] changes the expected number of DM halos by at most 1% within the redshift and mass ranges considered here. This difference has a negligible impact on the results of this work. The choice for using the EH transfer function is necessary for optimizing the CPU execution time of the Monte Carlo analyses (as described in section 4).

[3] In this section, we refer to DM halos instead of galaxy clusters because later we will introduce a mass proxy to properly build the likelihood for cluster abundance in terms of a cluster observable.

two likelihoods are equivalent under some conditions. The later will be employed to check if the cosmological parameter estimators are biased (for the considered sample sizes).

3.1 Poisson Distribution

The standard likelihood of the mean halo number counts is built assuming a Poisson distribution in bins of redshift and mass [1, 3, 10, 11, 13, 15, 36, 37], namely,

$$\mathcal{L}(\{\lambda_k(\{\theta_j\})\},\{n_k\}) = \prod_{k=1}^{\mathcal{N}} \frac{\lambda_k^{n_k} e^{-\lambda_k}}{n_k!}, \tag{3.1}$$

where $\mathcal{N}$ is the number of bins in the $\ln M - z$ space (or in the *mass-observable* - z space), n_k is the observed number of halos (clusters) in the k-th bin and the random variable $\lambda_k(\{\theta_j\})$ is the expected number of halos in the k-th bin for a given model.

In the regime where sample variance is negligible, a common practice is to take the limit where there is at most one halo per bin. In this case eq. (3.1) takes the form

$$\begin{aligned}\mathcal{L}(\{\lambda_k(\{\theta_j\})\},\{n_k\}) &= \prod_{k=1}^{n} \lambda_k e^{-\lambda_k} \prod_{l\neq k} e^{-\lambda_k} \\ &= \prod_{k=1}^{n} \lambda_k \prod_{all\ bins} e^{-\lambda_k},\end{aligned} \tag{3.2}$$

where now the first product is over the halos in the sample. The log likelihood is thus

$$\ln \mathcal{L}(\{\theta_j\},\{M_i,z_i\}) = \sum_{k=1}^{n} [\ln(\lambda_k(\{\theta_j\}))] - N(\{\theta_j\}), \tag{3.3}$$

where $\lambda_k(\{\theta_j\}) = \frac{d^2N(M_i,z_i,\{\theta_j\})}{dz d\ln M}$ (e.g. [3, 13]), $N(\{\theta_j\})$ is the predicted number of halos with redshift and mass values within, respectively, $[z_{min}, z_{max}]$ and $[M_{min}, M_{max}]$, and $\{\theta_j\}$ represents the set of cosmological parameters (it may also include other parameters such as those from a mass-observable relation).

3.2 Extended Maximum Likelihood

In this work, we introduce an unbinned likelihood [38] which we build following the extended maximum likelihood (EML) method [20, 21]. This approach does not require a normalized probability distribution, i.e., the number of events is not fixed. Particularly, the likelihood is the product of two terms. The first is the Poisson probability to find n halos in the whole mass and redshift ranges of the sample. The second term is the product of n terms, each one given by the probability distribution of a halo to have mass in the range $[M, M+dM]$ and to be found in the redshift interval $[z, z+dz]$, namely,

$$P(M,z,\{\theta_j\})dzdM = \frac{d^2N(M,z,\{\theta_j\})}{dz d\ln M}\frac{dz d\ln M}{N(\{\theta_j\})}, \tag{3.4}$$

where $N(\{\theta_j\})$ is the normalization factor.

Thus the likelihood function is

$$\mathcal{L}(\{\theta_j\},\{M_i,z_i\}) = \frac{N^n e^{-N}}{n!}\prod_{i=1}^{n}\frac{1}{N}\frac{d^2N(M_i,z_i,\{\theta_j\})}{dz d\ln M}, \tag{3.5}$$

where z_i is the redshift and M_i is the the mass of each halo. Therefore the log likelihood is

$$\ln \mathcal{L}(\{\theta_j\}, \{M_i, z_i\}) = \sum_{i=1}^{n} \ln \left(\frac{d^2 N(M_i, z_i, \{\theta_j\})}{dz d\ln M} \right) - N(\{\theta_j\}) - \ln n!. \tag{3.6}$$

Note that dropping the last term of eq. (3.6), since it does not depend on $\{\theta_j\}$, lead us to eq. (3.3). In this case the EML and Poisson methods are identical.

One advantage of the EML is the possibility to consider different informations for each cluster (such as mass-observable relations from different observables), since the likelihood is naturally a product of individual probabilities for each cluster. Also, the likelihood is naturally unbinned, such that it is free from possible bias that could be associated to the choice of the bin size. For this reason we will use the EML throughout this work. It is worth noting that, in ref. [6], the authors also build an unbinned likelihood using the truncated regression approach. Their likelihood is equivalent to eq. (3.6) except for a Poisson term of the number of missing objects N_{mis}, which is equal to unity when the likelihood is marginalized over N_{mis}.

4 Obtaining the bias of cosmological parameter estimators with the Monte Carlo method

The estimators for a given set of parameters ($\{\hat{\theta}_j\}$) are obtained by maximizing the likelihood with respect to these parameters. In order to analyse whether the estimators obtained from a likelihood function are biased, we need to calculate their expected values given a fiducial model $\{\theta_j^0\}$. The bias of $\hat{\theta}_j$ is defined as

$$b_{\hat{\theta}_j} = \langle \hat{\theta}_j \rangle - \theta_j^0. \tag{4.1}$$

The expected value of the cosmological parameter estimators cannot be computed analytically from the cluster number counts likelihood. To obtain $\langle \hat{\theta}_j \rangle$ we employ the Monte Carlo (MC) method, i.e., we generate a set of realizations of the cluster distribution in mass and redshift from a given input fiducial model and compute the best-fitting value of $\hat{\theta}_j$ for each realization by minimizing the likelihood function ($-2\ln\mathcal{L}$) [eq. (3.6)] with respect to θ_j. Assuming the probability distribution given by eq. (3.4), each realization is a catalog of DM halos containing their redshifts z_i and masses M_i (see appendix B for a detailed description). Then we compute the expected value using as an estimate the arithmetic mean $\overline{\hat{\theta}}_j$, i.e.,

$$\langle \hat{\theta}_j \rangle = \overline{\hat{\theta}}_j = \sum_{l=1}^{m} \frac{\hat{\theta}_{jl}}{m}, \tag{4.2}$$

where m is the number of realizations and $\hat{\theta}_{jl}$ is the best-fitting value for the l-th realization.

The variance of $\overline{\hat{\theta}}_j$ is given by

$$\sigma^2\left(\overline{\hat{\theta}}_j\right) = \frac{\sigma^2\left(\hat{\theta}_j\right)}{m}, \tag{4.3}$$

where $\sigma^2\left(\hat{\theta}_j\right)$ is the variance of the estimator $\hat{\theta}_j$. In cases where $b_{\hat{\theta}_j} \neq 0$, the significance of this bias is ensured by computing eq. (4.3). For example, if the estimator has a standard deviation of 1% in $\hat{\theta}_j^0$ and $b_{\hat{\theta}_j}$ is 5% of $\hat{\theta}_j^0$, then we must generate 100 realizations such that

$\sigma\left(\bar{\hat{\theta}}_j\right) = 0.1\%$ is one order smaller than $b_{\hat{\theta}_j}$. Note that this procedure usually requires a large number of realizations. In particular for our purposes, it is necessary to generate 10,000 realizations for each case, i.e., each choice of the fiducial model.

Therefore, to make this work feasible, it was necessary to develop numerical codes not only fast but whose framework could concatenate the different steps, i.e., generate a realization, build the likelihood, and perform the statistical analysis. Those algorithms are implemented in the NumCosmo library [24].

5 Bias from halo abundance likelihood

In this section, we apply the methodology described above to compute the bias of some cosmological parameter estimators in an idealized scenario where both the redshift and mass are perfectly known. For this, we have to adopt a fiducial model, which comprises both cosmological and survey parameters. Our choice is based on SZ surveys, since sample variance is usually negligible for their configurations. First, we assume a constant minimum mass threshold for the entire redshift interval. This is a good approximation for SZ surveys for which the mass limit for detection M_{min} is nearly redshift independent and is weakly dependent on cosmology [2, 39, 40]. Specifically, we set $M_{min} = 2 \times 10^{14} h^{-1} M_\odot$, which corresponds to the minimum value of the SZ observable that we will describe in section 6.

Besides the minimum mass threshold, we define a fiducial model by the redshift interval, the solid angle, and the set of cosmological parameters $\{\theta_j\}$. They are, respectively, $[0.3, 1.1]$, $\Delta\Omega = 720\text{deg}^2$ and

$$\begin{aligned}\{\theta_j\} &= \{\Omega_c, \Omega_b, H_0, n_s, \sigma_8, w_0\} \\ &= \{0.244, 0.0405, 73.9, 0.966, 0.766, -1\},\end{aligned} \tag{5.1}$$

where Ω_c is the cold dark matter density, Ω_b is the baryonic matter density ($\Omega_m = \Omega_c + \Omega_b$). The reason for choosing these specific values will become clear later in section 6.2.

Having defined the methodology to compute the bias of an estimator and the fiducial model, we now use them to determine whether the estimators are biased or not and if the biases obtained are relevant for cosmological studies. Throughout this paper, we focus our analyses on the estimators for Ω_c, σ_8, and w_0, since the first two are the cosmological parameters better constrained by cluster abundance (see, e.g., [1, 2]) and the later is the parameter used to probe the nature of dark energy, whose understanding is a major goal of ongoing and future surveys.

In this section, we study how the estimators' bias size vary with respect to the number of free parameters fitted. For this sake, we compute their biases fitting the respective estimators in one, two, and three-dimensional parametric spaces, i.e., (Ω_c), (σ_8), (w_0), (Ω_c, σ_8), (Ω_c, w_0), (σ_8, w_0), and $(\Omega_c, \sigma_8, w_0)$. The remaining parameters (cosmological and from the survey configurations) are always kept fixed.

Throughout this paper we report the bias on a parameter as a percentage of the 1σ error bar on this parameter. This helps to assess the significance of the bias in each case, i.e., even if the bias is large when compared to the estimated parameter values, it can be irrelevant if the error on this estimate is much larger. We define the following notation for the relative biases $B_{\hat{x}} \equiv b_{\hat{x}}/\sigma(\hat{x})$, i.e.,

$$B_{\hat{\Omega}_c} \equiv \frac{b_{\hat{\Omega}_c}}{\sigma(\hat{\Omega}_c)}, \quad B_{\hat{\sigma}_8} \equiv \frac{b_{\hat{\sigma}_8}}{\sigma(\hat{\sigma}_8)}, \quad B_{\hat{w}_0} \equiv \frac{b_{\hat{w}_0}}{\sigma(\hat{w}_0)},$$

DM halo abundance likelihood, $\Delta\Omega = 720\text{deg}^2$

Free	$\bar{\hat{\Omega}}_c \pm \sigma(\hat{\Omega}_c)$	$B_{\hat{\Omega}_c}$	$\bar{\hat{\sigma}}_8 \pm \sigma(\hat{\sigma}_8)$	$B_{\hat{\sigma}_8}$	$\bar{\hat{w}}_0 \pm \sigma(\hat{w}_0)$	$B_{\hat{w}_0}$
1	0.244 ± 0.011	3%	0.766 ± 0.006	2%	-1.00 ± 0.13	2%
2	0.246 ± 0.033	6%	0.766 ± 0.020	2%	$--$	$--$
2	0.253 ± 0.043	23%	$--$	$--$	-0.94 ± 0.46	12%
2	$--$	$--$	0.770 ± 0.022	20%	-0.98 ± 0.28	8%
3	0.239 ± 0.077	6%	0.777 ± 0.029	37%	-1.00 ± 0.63	$< 1\%$

Table 1. First Column: Number of fitted parameters. Even Columns: Estimated expected value of $\hat{x}$ and its standard deviation $\sigma(\hat{x})$ obtained fitting simultaneously 1 (first row), 2 (second, third, and forth rows), and 3 (last row) cosmological parameters and keeping the others fixed. Odd Columns: Bias size $b_{\hat{x}}$ relative to $\sigma(\hat{x})$.

where $b_{\hat{x}}$ is the bias of the estimator $\hat{x}$ computed using eqs. (4.1) and (4.2), and $\sigma(\hat{x})$ is the standard deviation of $\hat{x}$.

For each of the 7 parametric spaces defined above, we perform a MC with 10,000 realizations for the chosen fiducial model. This configuration provides an expected number about 80 clusters. The results for the mean values of the parameters, their variance, and their bias are shown in table 1. For a single free parameter the three estimators have small relative biases (about 2%). On the other hand, estimators in the bi-dimensional parametric spaces may have larger relative biases. For example, in the plane (Ω_c, w_0), $\hat{\Omega}_c$ has a relative bias of 23%. We also obtain a significant relative bias of 20% for $\hat{\sigma}_8$ when we fit this parameter together with w_0. For (Ω_c, σ_8), both estimators have small relative biases. In the three-dimensional parametric space, $\hat{\Omega}_c$ and $\hat{w}_0$ have small biases while $\hat{\sigma}_8$ has a relative bias of 37%. This case evinces the importance of knowing the properties of the cosmological parameter estimators.

6 Biases from cluster counts including a mass-observable relation

So far we presented a likelihood, a methodology, and a first analysis considering only DM halos. The relatively large biases found in the example above, in particular the significant bias obtained for $\hat{\sigma}_8$ in the case of 3 free parameters, pushes us to consider more realistic situations. A fundamental ingredient for modelling cluster abundance is to consider a mass proxy and associated mass-observable relation. Here we extend the formalism of the preceding sections to consider specifically the mass-observable relation for SZ surveys and take the fiducial values from SZ catalogs. We study how the relative biases change as a function of the number of parameters fitted and the size of the sample (changing both the area of the survey and the redshift depth).

6.1 Sunyaev–Zel'dovich mass-observable relation

One way to detect galaxy clusters and estimate their masses is through the SZ effect, which consists of a distortion in the frequency distribution of the cosmic microwave background photons due to inverse Compton scattering by the hot intracluster medium. The magnitude decrement due to the SZ effect (or increment for photons with frequencies $\gtrsim 217$ GHz) is a proxy for the mass of the cluster (see [16] and references therein).

In this work, we use the mass-observable relation developed by the SPT team in refs. [10–12], where the detection significance ξ is used as a SZ mass proxy [41]. In ref. [10] the authors obtained, using simulations, an unbiased significance ζ such that

$$\zeta = \sqrt{\langle\xi\rangle^2 - 3}, \tag{6.1}$$

and ξ is related to $\langle\xi\rangle$ by a Gaussian scatter of unit width, to which we will refer as $P(\xi|\zeta)$.

The scaling relation between ζ and M_{500} is given by [11, 12]

$$\zeta = A_{SZ}\left(\frac{M_{500}}{3\times10^{14}M_\odot h^{-1}}\right)^{B_{SZ}}\left(\frac{E(z)}{E(0.6)}\right)^{C_{SZ}}, \tag{6.2}$$

where A_{SZ} is the normalization, B_{SZ} is the slope, and C_{SZ} is the redshift evolution parameter. Following refs. [11, 12], we assume that $P(\ln\zeta|\ln M)$ is a Gaussian distribution with scatter given by D_{SZ}.

In section 3.2 we built the likelihood for halo abundance. Analogously, given the $\xi-M_{500}$ relation, we have that the likelihood for cluster number counts is

$$\ln\mathcal{L}(\{\theta_j\},\{\xi_i,z_i\}) = \sum_{i=1}^{n}\ln\left(\frac{d^2N(\xi_i,z_i,\{\theta_j\})}{dzd\xi}\right) - N(\{\theta_j\}) - \ln n!, \tag{6.3}$$

where

$$\frac{d^2N(\xi_i,z_i,\{\theta_j\})}{dzd\xi} = \int d\ln M\int d\zeta\frac{d^2N(M,z_i,\{\theta_j\})}{dzd\ln M}\,P(\xi_i|\zeta)\,P(\ln\zeta|\ln M). \tag{6.4}$$

Note that the normalization factor $N(\{\theta_j\})$ is now the expected number of clusters with $z_{min}\leq z\leq z_{max}$ and $\xi\geq\xi_{min}$. We assume that all objects with $\xi\geq\xi_{min}$ are detected in the entire redshift interval, i.e., the catalog is complete above this threshold.

6.2 Fiducial values from SPT

Now we shall apply the methodology of section 4 extending our analyses to include the SZ mass-observable relation, considering realistic parameters values taken from SZ surveys. The MC approach is performed by minimizing eq. (6.3) with respect to θ_j, assuming the probability distribution given by eq. (3.4) now in terms of ξ and the mass-observable relations $P(\xi|\zeta)$ and $P(\ln\zeta|\ln M)$. Each realization is now a catalog of clusters containing their redshifts z_i and the detection significance ξ_i (see appendix B for a discussion on the sampling).

In this case, the fiducial model used to generate the realizations also includes the parameters of the $\zeta - M_{500}$ relation and the minimum value of the detection significance ξ_{min}. Thus, along with the cosmological parameters, we have

$$\begin{aligned}\{\theta_j\} &= \{\Omega_c,\Omega_b,H_0,n_s,\sigma_8,w_0,A_{SZ},B_{SZ},C_{SZ},D_{SZ}\}\\ &=\{0.244,0.0405,73.9,0.966,0.766,-1,5.31,1.39,0.9,0.21\},\end{aligned} \tag{6.5}$$

and $\xi_{min}=5.0$. The redshift interval, $[0.3,1.1]$, and the threshold significance ξ_{min} are taken from the SPT catalog given in ref. [11]. The parameters $\{\theta_j\}$ correspond to the best-fit values obtained in this same reference by combining cluster abundance, Hubble parameter, and Big-Bang nucleosynthesis measurements, assuming a ΛCDM model.

Similarly to the analyses carried out in section 5, we compute the relative biases of $\hat{\Omega}_c$, $\hat{\sigma}_8$, and $\hat{w}_0$ in one, two, and three-dimensional parametric spaces. In section 5 we fixed

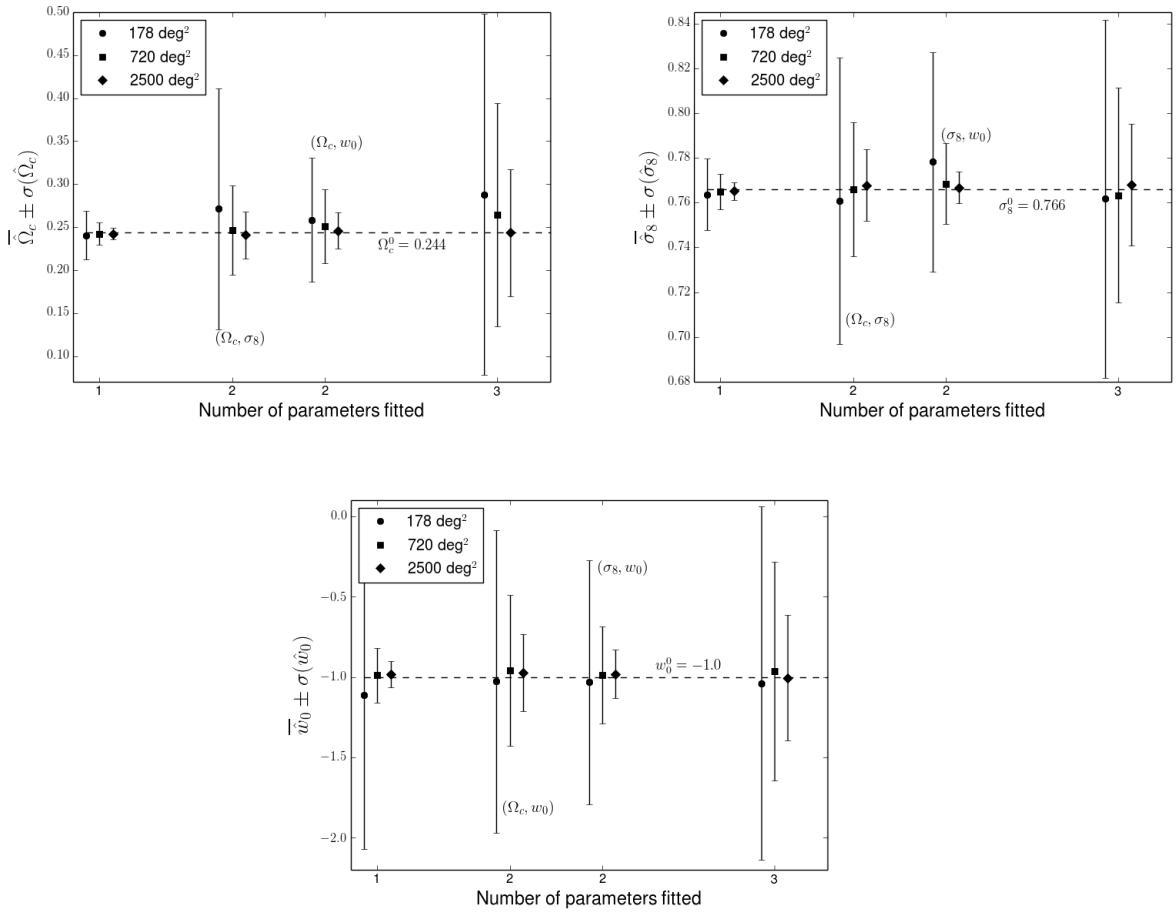

Figure 1. Expected values and error bars of the estimators $\hat{\Omega}_c$ (upper left panel), $\hat{\sigma}_8$ (upper right panel) and $\hat{w}_0$ (lower panel) computed for three different survey areas and the four parametric spaces probed. The dashed lines show the fiducial values.

$\Delta\Omega = 720\,\mathrm{deg}^2$, which is the area covered by the SPT catalog from ref. [12]. In this section we also consider $\Delta\Omega = 178$ [11] and $2500\,\mathrm{deg}^2$. The later being the total area covered by the SPT Survey [42]. Therefore, we are able to check how the estimator biases vary with the number of cosmological parameters being fitted simultaneously as well as with the size of the catalogs. As in section 5, all other parameters are kept fixed in the following analyses (including those from the mass-observable relation) and in each case we perform a MC with 10,000 realizations.

6.3 Dependence on the number of parameters fitted

The results for the several combinations of the parameters being fitted and the 3 values of the area discussed in the previous section are displayed in figure 1, which shows that the bias of the estimators are only a relatively small fraction of the size of the error bars.

In the one-dimensional parametric spaces the relative biases are generally greater than 10% but smaller than 25%. For both $\hat{\Omega}_c$ and $\hat{\sigma}_8$ the biases, $b_{\hat{\Omega}_c}$ and $b_{\hat{\sigma}_8}$, decrease with the increase of the survey area, as expected. Nevertheless, the errors bars $\sigma(\hat{\Omega}_c)$ and $\sigma(\hat{\sigma}_8)$ have a

steeper decrease, such that relative biases $B_{\hat{\Omega}_c}$ and $B_{\hat{\sigma}_8}$ end up increasing with the area. This shows that even for large samples, where one would expect the biases related to the cluster abundance likelihood to be smaller, this bias could still be a significant fraction of the error bars.

The freedom introduced by the increased number of fitted parameters results in larger error bars in almost all estimators, as expected. In general, the absolute biases $|b_{\hat{x}}|$ also increase with the number of fitted parameters. For the two and three-dimensional parametric spaces the relative biases, $B_{\hat{\Omega}_c}$ and $B_{\hat{w}_0}$ are roughly constant for both 178 and 720 deg^2. Namely, $B_{\hat{w}_0} \lesssim 10\%$ and $B_{\hat{\Omega}_c} \simeq 20\%$. On the other hand, $B_{\hat{\sigma}_8} \lesssim 10\%$ for the (Ω_c, σ_8) and $(\Omega_c, \sigma_8, w_0)$ spaces (being $< 1\%$ for the former space and 720 deg^2), while $B_{\hat{\sigma}_8} \simeq 25\%$ and 14% in the plane (σ_8, w_0) for 178 and 720 deg^2, respectively.

Only for $\Delta\Omega = 2500\,\mathrm{deg}^2$ we note a consistent decrease of the relative biases with the number of parameters fitted. In this case, all estimators present values for $B_{\hat{x}}$ of the order of 20%, 10%, and $< 10\%$ for one, two and three-dimensional parametric spaces, respectively.

6.4 Dependence on the survey area and depth

For most cases in the upper panels of figure 1 we see that the absolute values of the bias decrease with the area, as expected from the increase of the sample size. However, one may wonder if this trend continues for higher areas and whether the expected values converge to the fiducial values (it is worth mentioning that the sample size corresponding to 2500 deg^2 is of order of 250 objects). Therefore, we extend the analysis to larger areas and include also some intermediate values to see the general evolution scaling with area. In particular, in addition to the three areas of the previous section we run the MC simulations for $\Delta\Omega = 450, 1600, 3250,$ and 4000 deg^2. The later corresponds to the original planned SPT footprint [43]. This study is carried out only in the three-dimensional parametric space.

Figure 2 summarizes the results for the seven areas considered. We note that the three parameters present the larger absolute biases for the 3 smaller areas. The estimators are closer to their true values for 1600 ($\hat{\sigma}_8$) or 2500 deg^2 ($\hat{\Omega}_c$ and $\hat{w}_0$). Nevertheless, all estimators have their biases increased for the larger areas. In addition to displaying the values of the biases and the uncertainties in the parameters being fitted, in this figure we also show the uncertainties associated to the values of $b_{\hat{x}}$, i.e., $\sigma\left(\overline{\hat{x}}\right)$. We see that the biases are being precisely estimated.

To better understand the increase of the biases for larger areas, we also compute the estimators of the one- and three-dimensional parametric spaces for 10,000 and $40,000\mathrm{deg}^2$, being the last close to the full-sky limit. The results are displayed in table 2. The biases continue to grow with the increase of the area and, therefore, we have that $\hat{\Omega}_c$, $\hat{\sigma}_8$, and $\hat{w}_0$ are not consistent (i.e. $\lim_{n\to\infty} b_{\hat{x}} \neq 0$), in the sense that we are treating the full-sky area as the the asymptotic limit. We also note that the estimate of the expected value of all estimators computed in the one-dimensional parametric space have already converged for $10,000\,\mathrm{deg}^2$ (since $\overline{\hat{x}}$'s are equal for both areas), but not to their fiducial values, i.e., $b_{\hat{x}} \neq 0$. It is worth emphasizing that in the full-sky limit the bias is a dominant error source, being the relative biases about 30% to 50% for $(\Omega_c, \sigma_8, w_0)$ and about 80% for the one-dimensional parametric spaces.

In order to identify the cause of the *not consistent* feature of the cosmological parameter estimators, $\hat{\Omega}_c$, $\hat{\sigma}_8$, and $\hat{w}_0$, we carry out the MC analyses considering $40,000\,\mathrm{deg}^2$ and two other likelihoods: the halo abundance [given by eq. (3.6)] and a cluster abundance likelihood

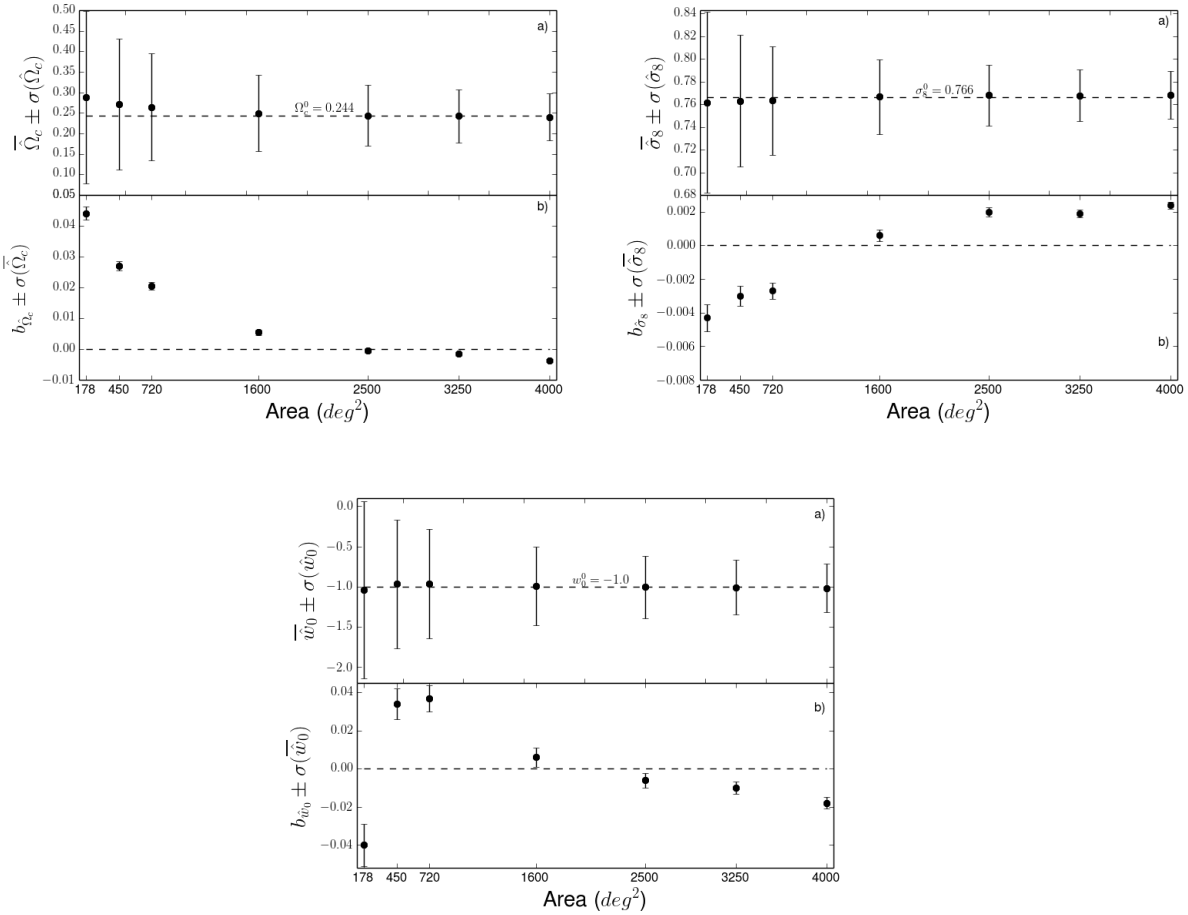

Figure 2. The expected values of the estimators (dots) are displayed with the error bars of the estimators (a) and of their means (b) for different survey areas.

$\xi - M_{500}$ cluster abundance likelihood, $z_{max} = 1.1$

$\Delta\Omega[\mathrm{deg}^2]$	Free	$\bar{\hat{\Omega}}_c \pm \sigma(\hat{\Omega}_c)$	$B_{\hat{\Omega}_c}$	$\bar{\hat{\sigma}}_8 \pm \sigma(\hat{\sigma}_8)$	$B_{\hat{\sigma}_8}$	$\bar{\hat{w}}_0 \pm \sigma(\hat{w}_0)$	$B_{\hat{w}_0}$
$10,000$	1	0.2425 ± 0.0036	42%	0.7653 ± 0.0021	33%	-0.983 ± 0.041	42%
	3	0.2367 ± 0.0351	21%	0.7690 ± 0.0133	23%	-1.026 ± 0.186	14%
$40,000$	1	0.2425 ± 0.0018	83%	0.7653 ± 0.0010	70%	-0.983 ± 0.021	81%
	3	0.2349 ± 0.0174	52%	0.7694 ± 0.0067	51%	-1.03 ± 0.09	33%

Table 2. First Column: Survey area. Second Column: Number of fitted parameters. Odd Columns: Estimated expected value of $\hat{x}$ and its standard deviation $\sigma(\hat{x})$ obtained fitting simultaneously 1 (first and third rows) and 3 (second and forth rows) cosmological parameters and keeping the others fixed. Even Columns: Bias size $b_{\hat{x}}$ relative to $\sigma(\hat{x})$.

given by

$$\ln \mathcal{L}(\{\theta_j\}, \{M_i^{obs}, z_i\}) = \sum_{i=1}^{n} \ln \left(\frac{d^2 N(M_i^{obs}, z_i, \{\theta_j\})}{dz d \ln M^{obs}} \right) - N(\{\theta_j\}) - \ln n!, \qquad (6.6)$$

where

$$\frac{d^2N(M_i^{obs}, z_i, \{\theta_j\})}{dz d\ln M^{obs}} = \int d\ln M \frac{d^2N(M, z_i, \{\theta_j\})}{dz d\ln M} P(\ln M^{obs}|\ln M), \tag{6.7}$$

and $P(\ln M^{obs}|\ln M)$ is a log-normal probability distribution for obtaining an observable mass M^{obs} given the true mass M,

$$P(\ln M^{obs}|\ln M)\, d\ln M^{obs} = \frac{1}{\sqrt{2\pi}\sigma_{\ln M}} e^{-\frac{\left(\ln M^{obs} - \ln M\right)^2}{2\sigma^2_{\ln M}}} d\ln M^{obs}, \tag{6.8}$$

with $\sigma_{\ln M} = D_{SZ}$. For both likelihoods, we obtain that all estimators are unbiased, i.e., the fiducial values are recovered within $\sigma\left(\hat{x}\right)$, such that the relative biases are less than 1%. Therefore, while the halo abundance likelihood provides biased estimators, when the sample size is small (see section 5), but is consistent, the $\xi - M_{500}$ cluster abundance likelihood yields biased estimators whose importance grows with the increase of the sample size. It is worth emphasizing that we cross-checked our code with the SPT team's one and, therefore, we discard the hypothesis that the results obtained with $\xi - M_{500}$ cluster abundance likelihood are due to bugs in the code.[4]

Besides the area, another factor that determines the sample size is the redshift depth. We therefore study the behavior of the bias and the statistical uncertainties as a function of the maximum redshift of the survey. In particular, we perform the MC analyses (using the $\xi - M_{500}$ cluster abundance likelihood) for seven values of the maximum redshift equally spaced in the interval $[0.9, 1.5]$. The later, $z_{max} = 1.5$, corresponds to the highest redshift of the SPT catalog in ref. [12].

Figure 3 shows the results considering $\Delta\Omega = 720\,\mathrm{deg}^2$ and the $(\Omega_c, \sigma_8, w_0)$ parametric space. The bias on $\hat{\Omega}_c$ decreases systematically with z_{max}, whereas $b_{\hat{\sigma}_8}$ decreases and then stays roughly constant after $z = 1.1$. Meanwhile, $b_{\hat{w}_0}$ presents an almost linear behavior as a function of z_{max} with its absolute value increasing after $z = 1.3$. In any case, as in the previous plots, the biases are not significant compared to the statistical error bars.

Finally, we study the estimators in the three-dimensional parametric space assuming $z_{max} = 1.5$ and $\Delta\Omega = 10,000$ and $40,000\,\mathrm{deg}^2$. Both absolute biases and the standard deviations are slightly smaller than those shown in table 2, such that $B_{\hat{x}}$ are essentially unaffected by the change in z_{max}.

6.5 Including photometric redshifts

The analyses carried out on the previous sections assumed perfect knowledge of the redshifts. However, spectroscopic redshifts are often available for only a fraction of the clusters, with many of them having z estimated photometrically. For example, 49 of 100 clusters from ref. [12] have just photometric measurements. We therefore include the uncertainties related to photometric redshifts in the likelihood for cluster number counts to verify its effect on the cosmological parameter estimators $\hat{\Omega}_c$, $\hat{\sigma}_8$, and $\hat{w}_0$.

For simplicity we assume that all clusters have the same Gaussian probability distribution for obtaining a photometric redshift z^{phot} given the true value z^{true},

$$P(z^{\mathrm{phot}}|z^{\mathrm{true}})dz^{\mathrm{phot}} = \sqrt{\frac{2}{\pi}} \frac{e^{-\frac{\left(z^{\mathrm{phot}} - z^{\mathrm{true}}\right)^2}{2\sigma_z^2}}}{\sigma_z(1 - \mathrm{erf}(z^{\mathrm{true}}/\sqrt{2\sigma_z^2}))} dz^{\mathrm{phot}}, \tag{6.9}$$

[4] The likelihood code of the SPT team is available at http://pole.uchicago.edu/public/data/reichardt12/index.html.

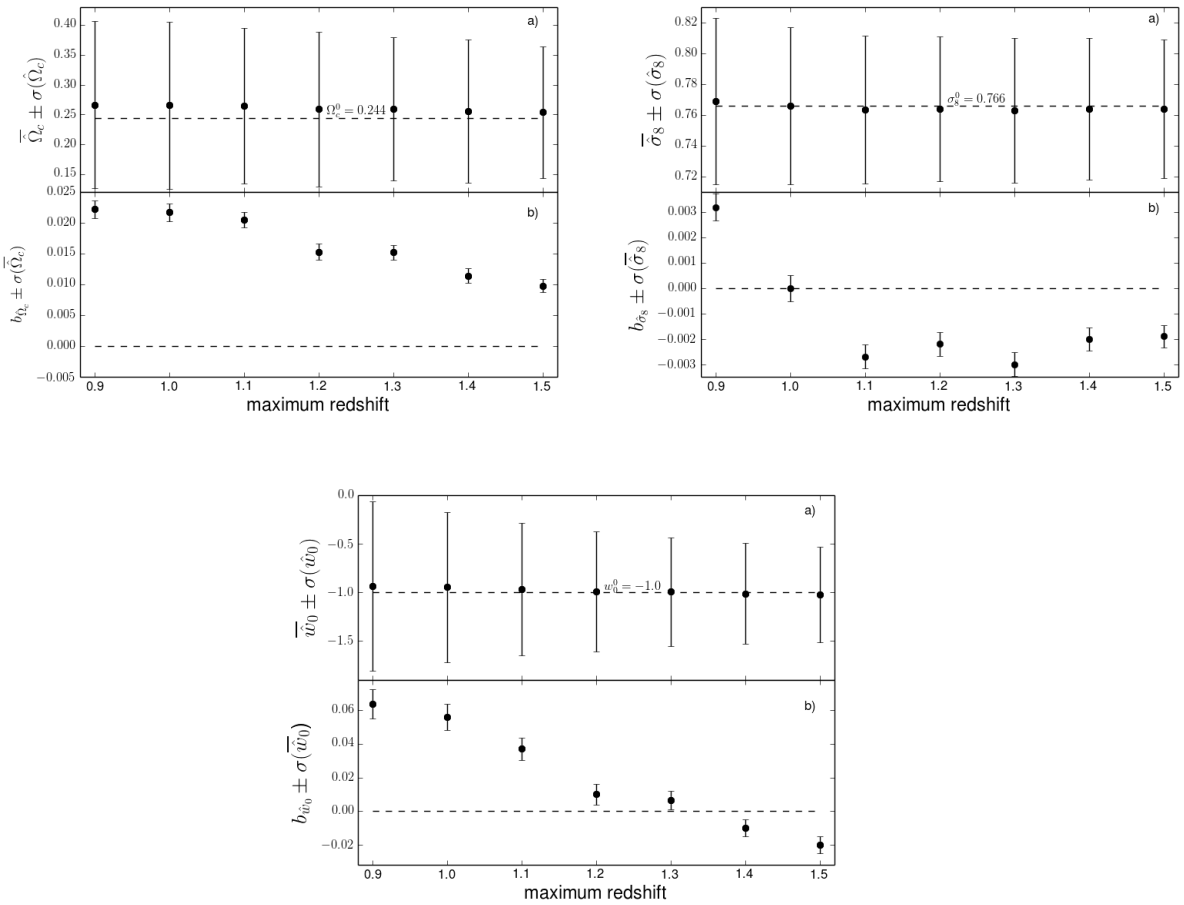

Figure 3. The expected values of the estimators (dots) are displayed with the error bars for the estimators (a) and for their means (b) as a function of z_{max}.

where $\sigma_z = \sigma_z^0(1+z)$, $\sigma_z^0 = 0.05$ and the normalization factor is obtained assuming $z^{\rm phot} > 0$.

Similarly to eqs. (6.3) and (6.4), we have

$$\ln \mathcal{L}(\{\theta_j\}, \{\xi_i, z_i^{\rm phot}\}) = \sum_{i=1}^{n} \ln\left(\frac{d^2N(\xi_i, z_i, \{\theta_j\})}{dz^{\rm phot} d\xi}\right) - N(\{\theta_j\}) - \ln n!, \tag{6.10}$$

where

$$\frac{d^2N(\xi_i, z_i^{\rm phot}, \{\theta_j\})}{dz^{\rm phot} d\xi} = \int dz^{\rm true} \int d\ln M \int d\zeta \, \frac{d^2N(M, z, \{\theta_j\})}{dz d\ln M} \times P(z_i^{\rm phot}|z^{\rm true})\, P(\xi_i|\zeta)\, P(\ln\zeta|\ln M), \tag{6.11}$$

and the normalization factor $N(\{\theta_j\})$ is now the expected number of clusters with $z_{min}^{\rm phot} \leq z^{phot} \leq z_{max}^{\rm phot}$ and $\xi \geq \xi_{min}$.

Now the MC approach is performed by minimizing eq. (6.10) with respect to θ_j and the sampling is carried out using the probability distribution given by eq. (6.11), the mass-observable relations, and $P(z^{\rm phot}|z^{\rm true})$. Each realization is now a catalog of clusters contain-

ing their photometric redshifts, $z_i^{\rm phot}$, and the detection significance, ξ_i (see appendix B). We study the three-dimensional parametric space for $z_{max} = 1.1$ and $\Delta\Omega = 720\,{\rm deg}^2$.

The results for the relative biases for the 3 parameters are shown in figure 4, together with other cases discussed in this work. We find that including the photometric redshift uncertainty has a negligible impact on the relative biases. The relative biases are $B_{\hat{\sigma}_c} = 17\%$, $B_{\hat{\Omega}_8} = 6\%$, and $B_{\hat{w}_0} = 8\%$, while the outcomes for the likelihood with only the mass-observable uncertainty give $B_{\hat{\sigma}_c} = 16\%$, $B_{\hat{\Omega}_8} = 6\%$ and $B_{\hat{w}_0} = 5\%$. Thought the biases do increase when considering photometry redshifts, the error bars also increase, keeping the ratio almost constant. For example, considering photometric redshifts we have $b_{\hat{w}_0} = 0.055$ and $\sigma(\hat{w}_0) = 0.72$, whereas considering perfect knowledge of the redshift yields $b_{\hat{w}_0} = 0.037$ and $\sigma(\hat{w}_0) = 0.68$.

7 Combination with other observables: CMB distance priors

So far we have studied estimators of three cosmological parameters computed using only the cluster abundance. However, in practice cosmological constraints are obtained combining cluster counts with other observables, such as the cosmic microwave background (CMB) radiation. Hence, in order to study more realistic estimators, we repeat the MC procedure including CMB data.

We do not consider the full CMB analysis since each case requires 10,000 realizations. Therefore, we build the CMB likelihood using only the so called distance priors (see [44] and references therein). They are dependent on the cosmological parameters and correspond to the redshift at decoupling $z_\star$, the location of the first acoustic peak l_A, and the shift parameter R.

The acoustic scale l_A is given by

$$l_A \equiv (1 + z_\star)\frac{\pi D_A(z_\star)}{r_s(z_\star)}, \tag{7.1}$$

where $D_A(z_\star)$ is the angular diameter distance and $r_s(z_\star)$ is the sound horizon size. The shift parameter is

$$R = \frac{\sqrt{\Omega_m H_0^2}}{c}(1 + z_*)D_A(z_*), \tag{7.2}$$

and the decoupling redshift is computed using the Hu & Sugiyama fitting formula [45].

The likelihood is

$$-2\ln L_{CMB} = \sum_{i,j}(x_i - d_i)\,(C_{ij})^{-1}\,(x_j - d_j), \tag{7.3}$$

where $x_i = (l_A, R, z_\star)$ and d_i are the distance prior values for a given realization (see below). In this work we use *Wilkinson Microwave Anisotropy Probe* 9-year (WMAP9) data, for which the inverse covariance matrix is given in ref. [46] as

$$(C_{ij})^{-1} = \begin{pmatrix} 3.182 & 18.253 & -1.429 \\ 18.253 & 11887.879 & -193.808 \\ -1.429 & -193.808 & 4.556 \end{pmatrix}.$$

We generate a realization for the CMB distance priors d_i assuming that they follow a Gaussian distribution with inverse covariance matrix $(C_{ij})^{-1}$ above and $(l_A, R, z_\star)$ calculated

from the fiducial model. Therefore, our MC simulations include both the realizations of the cluster distribution and the distance priors, and the likelihood minimized is a combination of eq. (7.3) and the cluster likelihood.

The results from the 10,000 MC realizations for the relative biases $B_{\hat{x}}$ for $\Delta\Omega = 720\,\mathrm{deg}^2$, $z_{max} = 1.1$, and the tridimensional parametric space $(\Omega_c, \sigma_8, w_0)$ are shown in figure 4, together with the other cases previously considered in this work. In the combination with the WMAP9 distance priors we consider two cases, including or not the photometric redshifts (always including the SZ mass-observable relation).

The combined likelihood provides a large improvement on both absolute biases and error bars for the Ω_c and w_0 estimators. Roughly, the error bars are 4 to 16 times smaller, depending on the parametric space, than those obtained using only the cluster likelihood. Assuming $\Delta\Omega = 720\,\mathrm{deg}^2$ and $z_{max} = 1.1$, we obtain that the biases for $\hat{w}_0$ and $\hat{\Omega}_c$ are small and compatible with zero within their own statistical error bars for the parametric spaces (w_0), (σ_8, w_0), and (Ω_c, σ_8). The relative biases also decrease in the (Ω_c, w_0) plane to $B_{\hat{\Omega}_c} \simeq 10\%$ and $B_{\hat{w}_0} \simeq 5\%$ in comparison to 17% and 9%, respectively, obtained with the cluster number counts likelihood only.

The MC results for 178, 720 and 2500 deg^2 and the three dimensional space $(\Omega_c, \sigma_8, w_0)$ reinforce that Ω_c is essentially constrained by CMB distance priors, since $\sigma(\hat{\Omega}_c) = 0.01$ and $B_{\hat{\Omega}_c} = 1\%$ for the first two cluster catalogs. We note a stronger weight of the cluster likelihood when $\Delta\Omega = 2500\,\mathrm{deg}^2$. Besides a decrease in the error bar, there is an increase in the absolute bias such that $B_{\hat{\Omega}_c} \simeq 8\%$. In the case of the w_0 estimators, the relative biases are $B_{\hat{w}_0} \lesssim 10\%$ for all sky areas, although the biases and error bars are now much smaller.

Differently from Ω_c and w_0, we note from figure 4 that σ_8 is almost insensitive to the CMB distance priors. The estimators obtained in (σ_8), (Ω_c, σ_8), and (σ_8, w_0) have the same bias and error bar than that from unidimensional space using the cluster abundance likelihood, namely $b_{\hat{\sigma}_8} = 0.001$ and $\sigma(\hat{\sigma}_8) = 0.008$, which gives $B_{\hat{\sigma}_8} \simeq 13\%$. In the bidimensional planes, this occurs because σ_8 is weakly correlated to Ω_c and w_0 ($Cor(\Omega_c, \sigma_8) \simeq -0.25$ and $Cor(\sigma_8, w_0) \simeq 0.09$). On the other hand, in the tridimensional parametric space, the strong correlations between these parameters increase their respective error bars such that $B_{\hat{\sigma}_8} \simeq 10\%$, 7%, and 3% for 178, 720 and 2500 deg^2, respectively.

Including photometric redshift uncertainty in the cluster abundance likelihood produces even smaller changes than those verified in section 6.5. Assuming $\Delta\Omega = 720\,\mathrm{deg}^2$, the error bars of the estimators obtained in $(\Omega_c, \sigma_8, w_0)$ space are basically equal to those without considering photometric uncertainty. The biases $b_{\hat{\sigma}_8}$ and $b_{\hat{w}_0}$ are slightly increased such that $B_{\hat{\sigma}_8} = 9\%$ and $B_{\hat{w}_0} = 6\%$, as illustrated in figure 4.

8 A comparison of methods to determine confidence contours

While the bias on cosmological parameter estimators needs to be evaluated with the Monte Carlo approach, the assessment of statistical errors can also be carried out using other methods such as Fisher matrix (FM) and profile likelihood (PL) (see also [1, 47, 48]). Therefore, it is worth comparing the error bars computed with these 3 different methodologies. In ref. [48], for example, the authors compare the confidence regions computed via FM and Markov Chain Monte Carlo (MCMC) using only a cluster abundance likelihood, as well with one combined with other observables.

In this section, we briefly review the FM and PL techniques and carry out some examples obtaining error bars and confidence regions for specific realizations.

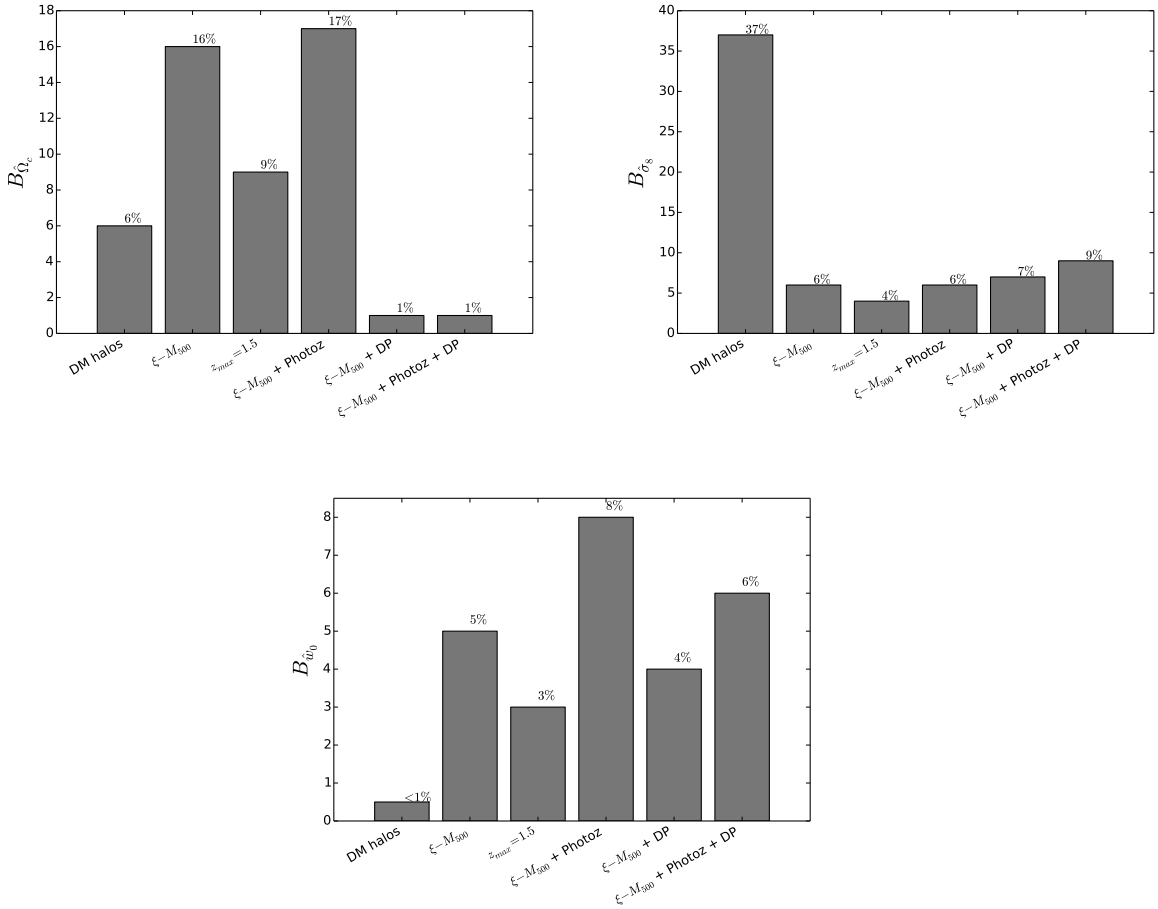

Figure 4. The relative biases of $\hat{\Omega}_c$ (left panel), $\hat{\sigma}_8$ (right panel), and $\hat{w}_0$ (lower panel), considering $\Delta\Omega = 720\,\mathrm{deg}^2$, $z_{max} = 1.1$, and the tridimensional parametric space $(\Omega_c, \sigma_8, w_0)$, obtained with the likelihood (left to right): DM halo abundance, cluster abundance (i.e. including the SZ mass-observable relation), extending the depth to $z_{max} = 1.5$, including photometric redshift uncertainty, combining with WMAP9 distance priors, with and without photometric redshifts, respectively.

8.1 Fisher Matrix

The Fisher matrix is defined as

$$F_{ij} = -\left\langle \frac{\partial^2 \ln \mathcal{L}(\vec{\theta})}{\partial\theta_i \partial\theta_j}\bigg|_{\vec{\theta}^0} \right\rangle . \tag{8.1}$$

If the estimators $\hat{\theta}_i$ are unbiased, then the FM is related with the variance of these estimators as (see ref. [22])

$$C(\hat{\theta}_i, \hat{\theta}_j) = C_{ij} \geq \left[-\left\langle \frac{\partial^2 \ln(L(\vec{\theta}))}{\partial\theta_i \partial\theta_j}\bigg|_{\vec{\theta}^0} \right\rangle \right]^{-1} , \tag{8.2}$$

where $C(\hat{\theta}_i, \hat{\theta}_j)$ are the elements of the covariance matrix. In practice it is assumed that the data set is sufficiently large and the second derivative of $\ln \mathcal{L}(\vec{\theta})$ computed at the best-fit $\hat{\theta}$

is a good estimator for the expected value and, therefore, $C_{ij} = (\hat{\mathbf{F}}^{-1})_{ij}$, where $\hat{\mathbf{F}}$ is a $n \times n$ matrix whose elements are $\hat{F}_{ij} = -\left.\frac{\partial^2 \ln(\mathcal{L}(\vec{\theta}))}{\partial\theta_i \partial\theta_j}\right|_{\hat{\vec{\theta}}}$. The size of the covariance matrix is defined by the number of parameters to be fitted. Say, for example, that we are fitting n parameters. Thus, the bidimensional contour (ellipse) of the i-th and j-th parameters is computed as [49]

$$\theta_i(t) = \hat{\theta}_i + q[a\cos(\alpha)\cos(t) - b\sin(\alpha)\sin(t)], \tag{8.3}$$

$$\theta_j(t) = \hat{\theta}_j + q[a\sin(\alpha)\cos(t) + b\cos(\alpha)\sin(t)], \tag{8.4}$$

where,

$$a^2 = \frac{C_{ii} + C_{jj}}{2} + \sqrt{\frac{(C_{ii} - C_{jj})^2}{4} + C_{ij}^2}, \tag{8.5}$$

$$b^2 = \frac{C_{ii} + C_{jj}}{2} - \sqrt{\frac{(C_{ii} - C_{jj})^2}{4} + C_{ij}^2}, \tag{8.6}$$

$$\tan(2\alpha) = \frac{2C_{ij}}{C_{ii} - C_{jj}}. \tag{8.7}$$

The confidence level is defined by q, namely, $q = 2.48$ corresponds to 2σ level. Since C_{ij} is the inverse of an $n \times n$ matrix, the other $n - 2$ parameters are marginalized over.

This technique is useful to forecast the constraints on cosmological parameters since it has low computational cost. However, the application of the FM method is limited as it provides just an approximation of the lower bound of the covariance matrix.

Although this methodology assumes that estimators are unbiased, we use it to reproduce what is usually done in the literature and then compare the results with MC and PL approaches. It is worth emphasizing that FM can also be obtained for biased estimators [50].

We begin the analyses computing the FM of the bi and tridimensional parametric spaces for 20 different realizations, considering the fiducial model with $\Delta\Omega = 720\,\mathrm{deg}^2$. In general, the FM errors bars are smaller than the those from MC. Only 2, 3, and 5 realizations resulted in larger error bars of w_0 in (σ_8, w_0), (Ω_c, w_0) and $(\Omega_c, \sigma_8, w_0)$, respectively. In all these cases, the best-fits were out of the 1σ confidence interval.

In order to compare the FM with the confidence region computed from MC approach, i.e., from the 10,000 realizations, we choose two realizations where the best-fit of the parameters are within the 1σ interval in all parametric spaces. The first realization, called *seed 125*,[5] provides error bars on the cosmological parameters smaller (roughly half) than the MC errors in all studied parametric spaces. The second realization, *seed 131*, gives similar error bars to those obtained with MC approach.

Figure 5 shows the results for the bidimensional case (Ω_c, w_0). In both panels, the orange dots represent the best-fits of the 10,000 realizations and the red lines are the 95.45% confidence regions from MC approach. We compute the MC contour using the quantile function from R Project for Statistical Computing.[6] The black lines are the FM 2σ bounds for seed 125 (left panel) and seed 131 (right panel) both computed using eq. (8.3). The FM contours are consistent with the MC result and, as expected, their sizes vary for each realization.

[5] We use the environment variable GSL_RNG_SEED of the GNU Scientific Library (url http://www.gnu.org/software/gsl/) to choose the seed to be used in NumCosmo to randomly generate a catalog.

[6] http://www.r-project.org/

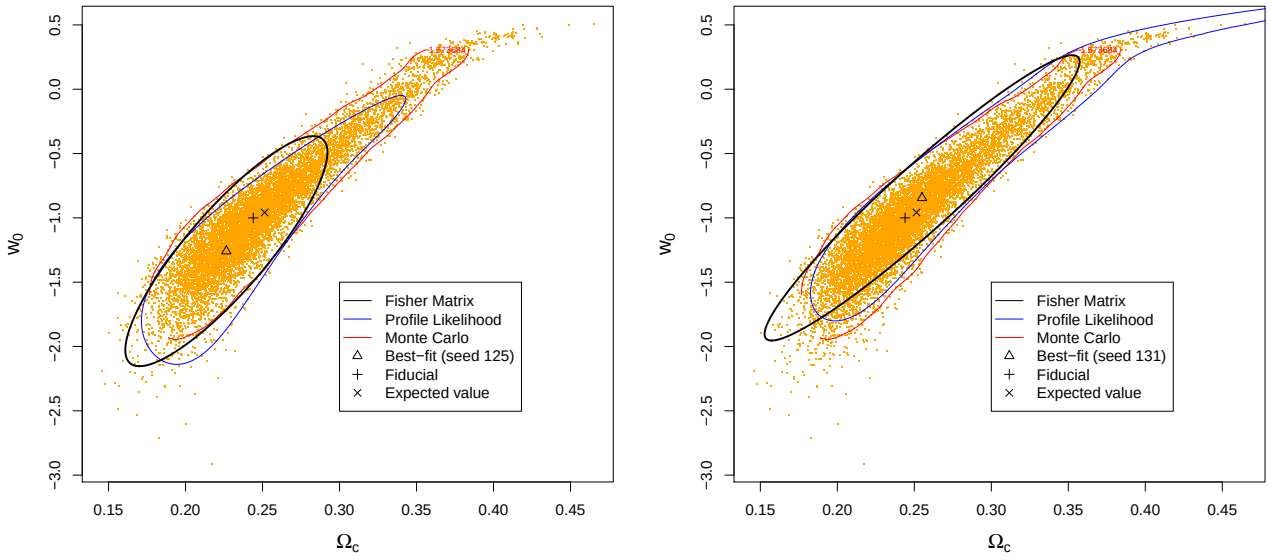

Figure 5. 2σ contour obtained from Monte Carlo approach (red line) and 2σ confidence regions for two specific realizations (left panel: seed 125 and right panel: seed 131) using Fisher matrix (black line) and profile likelihood (blue line) methods. The orange dots are the best-fits of 10000 realizations.

8.2 Profile Likelihood

The profile likelihood method consists in applying the likelihood ratio test [20, 51] to obtain the error bounds on the parameters. We define two nested models, i.e., a model with parameters $\{\theta_j\}$ and the same model where the parameters satisfy a set of n_r restrictions $f_a(\{\theta_j\}) = 0$. For each model we obtain the maximum likelihood estimators $\{\hat{\theta}_j\}$ and $\{\hat{\theta}_j^f\}$, where the last are the constrained ones. Note that, in general, these two sets are different. For the first we obtain the maximum of the likelihood with respect to all parameters whereas in the second we obtain the maximum enforcing the conditions $f_a(\{\theta_j\}) = 0$. In a simple example $f(\{\theta_j\}) = \theta_1 - \theta_1^0$, where θ_1^0 is a constant, the restriction is equivalent to keeping a parameter fixed to a constant value. Then, the likelihood ratio test is

$$\Lambda = \frac{L\left(\{\hat{\theta}_j^f\}, \{y_i\}\right)}{L\left(\{\hat{\theta}_j\}, \{y_i\}\right)}, \tag{8.8}$$

where $\{y_i\}$ is the data set. Under certain conditions, $-2\ln\Lambda$ is, asymptotically, a random variable described by a chi-square distribution of n_r degrees of freedom $\chi^2_{n_r}$ (Wilks' theorem) [20, 51].

Given the best-fit values $\{\theta_j^{\rm bf}\}$, we can use the test described above fixing a given parameter θ_k to a specific value θ_k^f to obtain the p-value associated with such choice. The p-value is defined as

$$1 - C = \int_{\chi^2_{n_r}}^{\infty} P_{n_r}(x)dx, \tag{8.9}$$

where $P_{n_r}(x)$ is the probability density of a chi-square distribution of n_r degrees of freedom and C is the confidence interval percentage, e.g., 68.27% (or 1σ for a Gaussian distribution).

Choosing a critical value C, we vary the value θ_j^f to find the interval within which this parameter is accepted for C. Thus, the bidimensional contour of θ_i and θ_j ($n_r = 2$) is obtained computing eq. (8.9), such that

$$\chi^2_{n_r=2} = -2\ln\left(\frac{L(\theta_i^f, \theta_j^f, \{\hat{\theta}_k^f\}, \{y_i\})}{L(\{\hat{\theta}_j^{\rm bf}\}, \{y_i\})}\right), \tag{8.10}$$

where the other parameters $\{\hat{\theta}_k^f\}$ can remain fixed or free. If $\{\theta_k^f\}$ are free, $\{\hat{\theta}_k^f\}$ are the best-fit values computed at $\left(\theta_i^f, \theta_j^f\right)$.

Similarly as done with FM method, we compute some confidence regions using PL. The dashed lines in figure 5 correspond to 2σ contour for seed 125 (left panel) and seed 131 (right panel). It is worth noting the ability of the PL technique in recovering some features, such as the shape, of the real distribution, in contrast to the FM, which, by construction, can only provide an ellipse. The bottom line is that both FM and PL contours are compatible with the MC result.

9 Conclusions

As has long been anticipated, cosmology has turned from a statistics to a systematics dominated field. Many sources of systematics have been considered in the literature, in particular those originated from observational effects and the modeling of the physical systems. In this work, we studied the biases from the properties of the estimator itself. Motivated by recent SZ surveys, for which the sample sizes are at most of the order of hundreds of objects and by the fact that ML methods can be biased for small samples (and even for large samples if the estimators are not consistent), we investigated the biases from an unbinned method for cluster number counts, which was shown to be equivalent to the now standard cluster abundance likelihood. The main aim of this work was to determine whether the biases found on some cosmological parameters were significant, as compared to their error bars.

To determine the biases from a given likelihood we have used the MC method, generating a large set of simulated samples and comparing the mean values of the cosmological parameters obtained by maximizing the likelihood to the fiducial models used in the simulations. This is computationally expensive and motivated the development of optimized codes that were incorporated in the NumCosmo library (see appendix A). The configurations used in the simulations (survey area, redshift range, cosmological parameters, etc.) were inspired by recent SZ surveys, in particular public catalogs from the SPT.

We first considered an idealized situation where the mass and redshift of the clusters are perfectly known, i.e. the DM halo abundance (section 5). In this case we found that the biases can be quite large for small samples. In particular we obtained a relatively large bias for σ_8, in the case where $\Delta\Omega = 720\,\mathrm{deg}^2$ and the likelihood is simultaneously fit for Ω_c, σ_8, and w_0, as compared to the expected (statistical) error bar on this parameter, yielding $B_{\hat{\sigma}_8} \sim 40\%$. On the other hand, we verified that $\hat{\Omega}_c$, $\hat{\sigma}_8$ and $\hat{w}_0$ are consistent when assuming the full-sky area.

We then considered a mass-observable (SZ) relation from SPT and found that the relative biases are significantly smaller, assuming typical areas of this survey (section 6.3). However, the relative biases can be as large as $\sim 25\%$ of the error bars for some configurations. Although the absolute values of the bias do in general decrease as the size of the sample increases, at

least for the smaller area samples, the statistical error bars also shrink. As a consequence, in these cases, the relative biases are less sensitive to the sample size.

To take a deeper look at the role of sample size, we obtained the biases as a function of both survey area and redshift depth, varying the 3 parameters, Ω_c, σ_8, and w_0 (section 6.4). The smaller absolute biases were obtained for $\Delta\Omega = 1,600$ and $2,500\,\mathrm{deg}^2$. For larger areas, we found out that the bias grows with the increase of the area. As the standard deviation of the estimators decreases, the relative biases become more relevant. In the full-sky limit, $B_{\hat{x}} \sim 80\%$ and $\sim 50\%$ for one- and three-dimensional parametric spaces, respectively. Therefore, we find that the estimators computed using $\xi - M_{500}$ cluster abundance likelihood are not consistent, differently from the those obtained with the halo abundance one. In particular, the biases can be a dominant error source as compared to the statistical errors due to shot-noise. However, other sources of error must be considered and it remains to be checked whether the bias found in this work will dominate in this case.

The sensitivity to z_{max} depends on the parameter under consideration. In any case, for all ranges probed, assuming $\Delta\Omega = 720\,\mathrm{deg}^2$, the biases are very small compared to the error bars. The situation is practically unchanged when we include photometric redshifts in the MC realizations and the likelihood (section 6.5).

Combining the cluster abundance likelihood with CMB distance priors (section 7) evinces that the later imposes strong constraints on Ω_c and w_0, significantly reducing the estimators' error bars in all parametric spaces. The bias is reduced in these cases, specially for Ω_c, since the CMB priors have more weight in this case and are assumed unbiased. On the other hand, since σ_8 is mostly determined by the cluster abundance, both its bias and statistical error bar are roughly unchanged.

Finally, we have compared the confidence regions of the fitted parameters obtained from the Fisher matrix and profile likelihood methods with the ones derived from the MC realizations and found that the former provide error bars that are broadly consistent with those from MC approach (section 8), further validating the use of these methods in the case of cluster abundance.

It is worth emphasizing that the results obtained are weakly sensitive to the values of the fiducial cosmological model. For example, we used also $\Omega_c = 0.15$, $\sigma_8 = 0.85$, and $w_0 = -0.85$ and found very similar results.

For optical surveys, such as SDSS, DES and LSST, this study must consider sample variance in the cluster likelihood function. Since sample variance dominates the Poisson term for large galaxy clusters samples, we expect that the cosmological parameter estimators would have smaller biases in this context, provided that the sample variance estimator is unbiased.

In general, the mass-observable (M-O) relations are sources of systematic errors in the inference of cosmological parameters. A common approach to minimize the effect of these errors while also constraining the M-O relation is to combine other observables and to fit the cosmological parameters along with those of the M-O relation (so-called self-calibration). Therefore, as future work, we plan to extend this study and obtain the estimators of both type of parameters using, for example, cluster, CMB and type Ia supernovae data. As a preliminary analysis, we used the cluster abundance likelihood and computed the estimators of the two-dimensional parametric spaces, (Ω_c, D_{SZ}), (σ_8, D_{SZ}) and (w_0, D_{SZ}), assuming $720\,\mathrm{deg}^2$. Following ref.[11], we considered a Gaussian prior on D_{SZ} with mean equal to 0.21 and standard deviation 0.16. In this case, the cosmological parameters are moderately correlated (anti-correlated) to D_{SZ}, $Cor(\hat{x}, D_{SZ}) \simeq \pm 0.5$. Except for $\hat{\Omega}_c$ and $\hat{\sigma}_8$, whose relative biases are about 20%, the other estimators have negligible relative biases ($< 5\%$).

If on one hand we obtained that in general $B_{\hat{x}} \lesssim 10\%$ for the most realistic cases of SZ surveys (considering typical areas of SPT), on the other hand we have shown that the consistent feature of the estimators depends on the modeling of the M-O relation and, when this property is not fulfilled, the bias of the estimators cannot be neglected for very large areas.

The results of this work validate the use of the current maximum likelihood methods for present SZ surveys (small catalogs). However, they highlight the need for further studies for upcoming wide-field sensitive surveys, since biases from SZ estimators do not go away with increasing sample sizes and they may become the dominant source of error for an large area survey, as the Planck probe, and sensitive as the SPT and ACT.

Acknowledgments

MPL acknowledges CAPES (grant PRODOC 2712/2010) and CNPq (PCI/MCTI/CBPF and PCI/MCTI/INPE programs) for financial support. MM is partially supported by CNPq (grant 309804/2012-4) and FAPERJ (grant E-26/110.516/2012). MPL is grateful to Sandro Vitenti for valuable discussions and comments. The authors thank Fernando de Simoni, Juan Estrada, and Scott Dodelson for useful suggestions. The authors also thank the anonymous referee for the careful reading of this work and valuable suggestions. This work made use of the CHE cluster, managed and funded by ICRA/CBPF, with financial support from FINEP and FAPERJ.

A Numerical Cosmology Library (NumCosmo)

In this appendix we present a summary and a short description of each object used in this work. The NumCosmo library is a free library written in the C language dedicated to numerical calculations in cosmology [24]. The documentation and examples are available at the project's url.

In section 2 we introduced the cosmological model to compute the expected halo number counts. This calculation was split in several objects to allow for each step to be modified for different modeling or optimization. These objects are listed below,

- NcMatterVar: the filtered matter variance for a given window function [eq. (2.5)].
- NcTransferFunc: the transfer function $T(k)$ [eq. (2.7)].
- NcGrowthFunc: the growth function [eq. (2.9)].
- NcWindowFunc: the window function [eq. (2.6)].
- NcMassFunc: the mass function [eq. (2.4)].
- NcMultiplicity: the multiplicity function [eq. (2.10)].

The NumCosmo's object that implements the sampling method, described in appendix B, is NcDataClusterNCount. This object is also used to calculate the abundance likelihood described in eqs. (3.6), (6.3), and (6.10). The mass-observable relation and photometric redshift distribution objects are implementations of NcClusterMass and NcClusterRedshift, respectively. In this work we used the implementations NcClusterMassBenson and NcClusterPhotozGaussGlobal. The WMAP distance priors described in section 7 are implemented by the NcDataCMBDistPriors object for both sampling and likelihood evaluation.

To obtain the results from Fisher Matrix, Monte Carlo, and profile likelihood approaches (Secs. 8.1 and 8.2, respectively), we used the objects NcmFit for both FM and MC and NcmLHRatio1d for the profile likelihood method.

It is worth emphasizing that, differently from most works, we do not make a grid in redshift and observable quantities, such as ξ, to compute eq. (6.4) [or eq. (6.11)] and, thus, the confidence regions. We calculate these equations at each point (ξ_i, z_i).

B Sampling

In this appendix we describe the procedure to generate the realizations of the samples $\{\xi_i, z_i\}$. First we compute the halo abundance $N(\{\theta_j\})$ given a fiducial model,

$$N(\{\theta_j^0\}) = \int_{z_{min}}^{z_{max}} dz \int_{\ln M_{min}}^{\infty} d\ln M \, \frac{d^2N(\ln M, z)}{dz d\ln M}, \tag{B.1}$$

where $\ln M_{min}$ is obtained from eqs. (6.1) and (6.2). Using $N(\{\theta_j^0\})$ as the mean of a Poisson distribution, we randomly generate the total number of objects n.

The second step consists in creating a sample with n redshift values z_i from the probability distribution of finding a halo with mass greater than $M_{\rm min}$ and in the redshift interval $[z, z + dz]$, i.e.,

$$\mathcal{P}(z)dz = \frac{1}{N(\{\theta_j\})}\left(\frac{dN}{dz}\right)dz, \tag{B.2}$$

where $N(\{\theta_j\})$ is the normalization factor. To generate the set $\{z_i\}$ following this distribution we employ the inverse transform sampling, which we briefly describe below. First we define the cumulative

$$f(z) = \int_0^z \mathcal{P}(z')dz', \tag{B.3}$$

since $f(z)$ is a monotonically increasing function whose image is $[0, 1]$, there is a one-to-one relation between z and $f(z)$. Given also that $f(z)$ is a random variable with uniform distribution over $[0, 1]$, we generate n random numbers $\{u_i\}$ from a uniform distribution and inverted equation (B.3) obtaining $z(f)$ and, therefore, the set $\{z_i\} = \{z(u_i)\}$.

For each value of z_i generated, we obtain a value M_i from the conditional distribution of obtaining a halo with mass in the range M and $M + dM$ given z_i, defined as

$$P(M|z_i) = \frac{P(M, z_i)}{\mathcal{P}(z_i)}, \tag{B.4}$$

where $P(M, z_i)$ is given by eq. (3.4) and $\mathcal{P}(z_i)$ by eq. (B.2). Then we use the cumulative

$$f(M|z_i) = \int_0^M P(M'|z_i)dM' \tag{B.5}$$

to define $M(f, z_i)$ and thus we employ the same procedure described above to get $\{z_i\}$, but now obtaining $\{M_i, z_i\}$.

Finally, to obtain the cluster sample $\{\xi_i, z_i\}$ (to which we refer as a realization of the cluster distribution), a value ζ_i is randomly generated from the Gaussian distribution $P(\ln\zeta|\ln M)$ with scatter D_{SZ} and mean given by the logarithm base e of eq. (6.2), where M_{500} is the true halo mass M_i. Then we randomly generate ξ_i using the Gaussian distribution $P(\xi|\zeta)$ with

scatter equal to one and mean obtained substituting ζ_i in eq. (6.1). As the last step, we select the objects which fulfill the condition $\xi \geq \xi_{min}$.

In section 6.5 we also included the photometric redshift uncertainty. Therefore, the realization $\{\xi_i, z_i^{phot}\}$ is obtained from the sample $\{\xi_i, z_i\}$ described above where z_i^{phot} is randomly generated from eq. (6.9). As done for ξ_i, the generated values are selected such that $z_{min} \leq z_i^{phot} \leq z_{max}$.

References

[1] G. Holder, Z. Haiman, and J. J. Mohr, *Constraints on ω_m, ω_λ, and σ_8 from galaxy cluster redshift distributions*, *ApJ* **560** (2001) L111.

[2] Z. Haiman, J. J. Mohr, and G. P. Holder, *Constraints on cosmological parameters from future galaxy cluster surveys*, *ApJ* **553** (2001) 545.

[3] S. Borgani, P. Rosati, P. Tozzi, S. A. Stanford, P. R. Eisenhardt, C. Lidman, B. Holden, R. Della Ceca, et al., *Measuring Ω_m with the rosat deep cluster survey*, *ApJ* **561** (2001) 13.

[4] D. Huterer and M. White, *Weak lensing as a calibrator of the cluster mass-temperature relation*, *ApJ* **578** (2002) 95.

[5] A. Vikhlinin, A. V. Kravtsov, R. A. Burenin, H. Ebeling, W. R. Forman, A. Hornstrup, C. Jones, S. S. Murray, et al., *Chandra cluster cosmology project iii: Cosmological parameter constraints*, *ApJ* **692** (2009) 1060 [arXiv:0812.2720].

[6] A. Mantz, S. W. Allen, D. Rapetti, and H. Ebeling, *The observed growth of massive galaxy clusters - i. statistical methods and cosmological constraints*, *Mon. Not. R. Astron. Soc.* **406** (2010) 1759 [arXiv:0909.3098].

[7] S. W. Allen, A. E. Evrard, and A. B. Mantz, *Cosmological parameters from observations of galaxy clusters*, *ARA&A* **49** (2011) 409 [arXiv:1103.4829].

[8] T. Abbott, G. Aldering, J. Annis, et al., *The dark energy survey*, (2005) [astro-ph/0510346].

[9] L. D. E. S. Collaboration, *Large synoptic survey telescope: Dark energy science collaboration*, (2012) [arXiv:1211.0310].

[10] K. Vanderlinde, T. M. Crawford, T. de Haan, J. P. Dudley, L. Shaw, P. A. R. Ade, K. A. Aird, B. A. Benson, et al., *Galaxy clusters selected with the sunyaev-zel'dovich effect from 2008 south pole telescope observations*, *ApJ* **722** (2010) 1180 [arXiv:1003.0003].

[11] B. A. Benson, T. de Haan, J. P. Dudley, C. L. Reichardt, K. A. Aird, K. Andersson, R. Armstrong, M. L. N. Ashby, et al., *Cosmological constraints from sunyaev-zel'dovich-selected clusters with x-ray observations in the first 178 deg^2 of the south pole telescope survey*, *ApJ* **763** (2013) 147 [arXiv:1112.5435].

[12] C. L. Reichardt, B. Stalder, L. E. Bleem, T. E. Montroy, K. A. Aird, K. Andersson, R. Armstrong, M. L. N. Ashby, et al., *Galaxy clusters discovered via the sunyaev-zel'dovich effect in the first 720 square degrees of the south pole telescope survey*, *ApJ* **763** (2013) 127 [arXiv:1203.5775].

[13] N. Sehgal, H. Trac, V. Acquaviva, P. A. R. Ade, P. Aguirre, M. Amiri, J. W. Appel, L. F. Barrientos, et al., *The atacama cosmology telescope: Cosmology from galaxy clusters detected via the sunyaev-zel'dovich effect*, *ApJ* **732** (2011) 44 [arXiv:1010.1025].

[14] P. Collaboration, P. A. R. Ade, N. Aghanim, C. Armitage-Caplan, M. Arnaud, M. Ashdown, F. Atrio-Barandela, J. Aumont, C. Baccigalupi, et al., *Planck 2013 results. xx. cosmology from sunyaev-zeldovich cluster counts* [arXiv:1303.5080].

[15] A. Vikhlinin, R. A. Burenin, H. Ebeling, W. R. Forman, A. Hornstrup, C. Jones, A. V. Kravtsov, S. S. Murray, et al., *Chandra cluster cosmology project. ii. samples and x-ray data reduction*, *ApJ* **692** (2009) 1033 [arXiv:0805.2207].

[16] S. Giodini, L. Lovisari, E. Pointecouteau, S. Ettori, T. H. Reiprich, and H. Hoekstra, *Scaling relations for galaxy clusters: Properties and evolution*, *Space Sci. Rev.* **177** (2013) 247 [arXiv:1305.3286].

[17] M. Sahlén, P. T. P. Viana, A. R. Liddle, A. K. Romer, M. Davidson, M. Hosmer, E. Lloyd-Davies, K. Sabirli, et al., *The xmm cluster survey: forecasting cosmological and cluster scaling-relation parameter constraints*, *MNRAS* **397** (2009) 577 [arXiv:0802.4462].

[18] M. Shimon, N. Itzhaki, and Y. Rephaeli, *Bias-limited extraction of cosmological parameters*, *JCAP* **3** (2013) 9 [arXiv:1212.0797].

[19] R. Lupton, *Statistics in Theory and Practice*. Princeton Univ. Press, 1993.

[20] G. Cowan, *Statistical Data Analysis*. Oxford University Press, 1998.

[21] R. J. Barlow, *Statistics: A guide to the use of statistical methods in the physical sciences*. The Manchester Physics Series. John Wiley & Sons, 1999.

[22] H. J. Bierens, *Introduction to the Mathematical and Statistical Foundations of Econometrics*. Cambridge University Press, 2005.

[23] W. Hu and A. V. Kravtsov, *Sample variance considerations for cluster surveys*, *ApJ* **584** (2003) 702.

[24] S. D. P. Vitenti and M. Penna-Lima, *Numerical Cosmology – NumCosmo*, *http://www.nongnu.org/numcosmo/* (2012).

[25] W. H. Press and P. Schechter, *Formation of galaxies and clusters of galaxies by self-similar gravitational condensation*, *ApJ* **187** (1974) 425.

[26] J. R. Bond, S. Cole, G. Efstathiou, and N. Kaiser, *Excursion set mass functions for hierarchical gaussian fluctuations*, *ApJ* **379** (1991) 440.

[27] R. K. Sheth and G. Tormen, *Large scale bias and the peak background split*, *MNRAS* **308** (1999) 119.

[28] D. J. Eisenstein and W. Hu, *Baryonic features in the matter transfer function*, *ApJ* **496** (1998) 605 [astro-ph/9709112].

[29] A. Lewis, A. Challinor, and A. Lasenby, *Efficient computation of CMB anisotropies in closed FRW models*, *ApJ* **538** (2000) 473 [astro-ph/9911177].

[30] J. P. Uzan, *The acceleration of the universe and the physics behind it*, *Gen. Rel. Grav.* **39** (2007) 307.

[31] S. Nesseris and L. Perivolaropoulos, *Testing λCDM with the growth function $\delta(a)$: Current constraints*, *Phys. Rev. D* **77** (2008) 023504.

[32] A. Jenkins, C. S. Frenk, S. D. M. White, J. M. Colberg, S. Cole, A. E. Evrard, H. M. P. Couchman, and N. Yoshida, *Mass function of dark matter halos*, *MNRAS* **321** (2001) 372.

[33] M. Warren, K. Abazajian, D. E. Holz, and L. Teodoro, *Precision determination of the mass function of dark matter halos*, *ApJ* **646** (2006) 881.

[34] J. Tinker, A. V. Kravtsov, A. Klypin, K. Abazajian, M. Warren, G. Yepes, S. Gottlöber, and D. E. Holz, *Toward a halo mass function for precision cosmology: The limits of universality*, *ApJ* **688** (2008) 709.

[35] C. E. Cunha and A. E. Evrard, *Sensitivity of galaxy cluster dark energy constraints to halo modeling uncertainties*, *Phys. Rev. D* **81** (2010) 083509 [arXiv:0908.0526].

[36] W. Cash, *Parameter estimation in astronomy through application of the likelihood ratio*, *ApJ* **228** (1979) 939.

[37] E. Rozo, R. H. Wechsler, E. S. Rykoff, J. T. Annis, M. R. Becker, A. E. Evrard, J. A. Frieman, S. M. Hansen, et al., *Cosmological constraints from the sdss maxbcg cluster catalog*, *ApJ* **708** (2010) 645 [arXiv:0902.3702].

[38] M. Penna-Lima, *Abundância de Aglomerados de Galáxias como Observável Cosmológico: Aplicações aos Levantamentos Fotométricos DES e SDSS*, *PhD Thesis*, Centro Brasileiro de Pesquisas Físicas (2010) [pdf].

[39] J. E. Carlstrom, M. K. Joy, L. Grego, G. P. Holder, W. L. Holzapfel, J. J. Mohr, S. Patel, and E. D. Reese, *Imaging the sunyaev-zel'dovich effect*, *PhST* **85** (2000) 148.

[40] G. P. Holder, J. J. Mohr, J. E. Carlstrom, A. E. Evrard, and E. M. Leitch, *Expectations for an interferometric sunyaev-zeldovich effect survey for galaxy clusters*, *ApJ* **544** (2000) 629.

[41] Z. Staniszewski, P. A. R. Ade, K. A. Aird, B. A. Benson, L. E. Bleem, J. E. Carlstrom, C. L. Chang, H. M. Cho, et al., *Galaxy clusters discovered with a sunyaev-zel'dovich effect survey*, *ApJ* **701** (2009) 32 [arXiv:0810.1578].

[42] K. T. Story, C. L. Reichardt, Z. Hou, R. Keisler, K. A. Aird, B. A. Benson, L. E. Bleem, J. E. Carlstrom, et al., *A measurement of the cosmic microwave background damping tail from the 2500-square-degree spt-sz survey*, *ApJ* **779** (2013) 86 [arXiv:1210.7231].

[43] J. Ruhl, P. A. R. Ade, J. E. Carlstrom, H.-M. Cho, T. Crawford, M. Dobbs, C. H. Greer, N. w. Halverson, et al., *The south pole telescope*, *SPIE Conference Series* (C. M. Bradford, P. A. R. Ade, J. E. Aguirre, J. J. Bock, M. Dragovan, L. Duband, L. Earle, J. Glenn, H. Matsuhara, B. J. Naylor, H. T. Nguyen, M. Yun, and J. Zmuidzinas, eds.), of *SPIE* **5498** (2004) 11.

[44] E. Komatsu, K. M. Smith, J. Dunkley, C. L. Bennett, B. Gold, G. Hinshaw, N. Jarosik, D. Larson, et al., *Seven-year wilkinson microwave anisotropy probe (wmap) observations: Cosmological interpretation*, *ApJS* **192** (2011) 18 [arXiv:1001.4538].

[45] W. Hu and N. Sugiyama, *Small scale cosmological perturbations: An analytic approach*, *ApJ* **471** (1996) 542 [astro-ph/9510117].

[46] G. Hinshaw, D. Larson, E. Komatsu, D. N. Spergel, C. L. Bennett, J. Dunkley, M. R. Nolta, M. Halpern, et al., *Nine-year wilkinson microwave anisotropy probe (wmap) observations: Cosmological parameter results*, *ApJS* **208** (2013) 19 [arXiv:1212.5226].

[47] L. Wolz, M. Kilbinger, J. Weller and T. Giannantonio, *On the validity of cosmological Fisher matrix forecasts*, *JCAP* **9** (2012) 009 [arXiv:1205.3984].

[48] S. Khedekar and S. Majumdar, *Cosmology with the largest galaxy cluster surveys: going beyond Fisher matrix forecasts*, *JCAP* **2** (2013) 030 [arXiv:1210.5586].

[49] D. Coe, *Fisher matrices and confidence ellipses: A quick-start guide and software*, (2009) [arXiv:0906.4123].

[50] Z. Ben-Haim and Y. C. Eldar, *On the constrained Cramér - Rao bound with a singular fisher information matrix*, *IEEE Signal Processing Letters* **16** (2009) 453.

[51] P. G. Hoel, *Introduction to Mathematical Statistics*. John Wiley & Sons, 1966.